

Multilayered electronic transfer tattoo that can enable the crease amplification effect

Lixue Tang^{1,2}, Jin Shang³, Xingyu Jiang^{1*}

Electronic tattoos have great potential in health and movement sensing applications on the skin. However, existing electronic tattoos cannot be conformal, sticky, and multilayered at the same time. Here, we have achieved multilayered integration of the electronic tattoo that is highly stretchable (800%), conformal, and sticky. This electronic tattoo can enable the crease amplification effect, which can amplify the output signal of integrated strain sensors by three times. The tattoo can be transferred to different surfaces and form a firm attachment, where no solvent or heat is needed. The tattoo fabrication is straightforward and scalable; a layer-by-layer strategy and two materials (metal-polymer conductors and the elastomeric block copolymer) are used to fabricate the circuit module with desirable numbers of layers within the tattoo. A three-layered tattoo integrating 1 heater and 15 strain sensors is developed for temperature adjustment, movement monitoring, and remote control of robots.

Copyright © 2021
The Authors, some
rights reserved;
exclusive licensee
American Association
for the Advancement
of Science. No claim to
original U.S. Government
Works. Distributed
under a Creative
Commons Attribution
NonCommercial
License 4.0 (CC BY-NC).

INTRODUCTION

Wearable/implantable devices that can seamlessly integrate with human tissues will greatly improve the quality of life by real-time health monitoring and treatment (1–8). Wearable/implantable devices are usually compatible with human tissues such as the skin, brain, and heart due to their soft substrates (1, 6, 9–15). Most of the reported wearable devices are based on silicone substrates (16–21), because such substrates are flexible and stretchable and have a similar modulus to human tissues. Also, they are chemically inert and will not cause damage to human tissues. However, such silicone-based wearable devices cannot form a firm attachment to human tissues. Deformations on human tissues will partially or entirely detach the silicone-based devices from tissues, causing an unstable interface between human tissues and devices. External supports are needed to fix wearable devices to tissues. To achieve a stable connection between the skin and the devices, some of the wearable devices are fabricated into electronic tattoos that can firmly attach to the skin and deform with the skin (22–30). However, the current electronic tattoos are usually obtained by directly printing electronic circuits on the skin (25, 27, 28) or commercial transfer tattoos (26, 29). Electronic circuits in tattoos fabricated by such strategies are single-layered, which cannot achieve circuits with multiple functions. There will be an inevitable overlap of the interconnects when it comes to complex circuits. Besides, for commercial transfer tattoos, solvents are usually required to transfer onto the skin. Multilayered wearable devices typically have a large thickness (>100 μm) (19, 20, 31, 32), which cannot be conformal with small features such as fingerprints and finger joint folds/creases on the skin. As a result, existing wearable devices cannot be attachable, crease conformal, and multilayered simultaneously. Here, to balance those incompatibilities, we developed the multilayered electronic transfer tattoo (METT). The METT can be embedded into small features (finger creases and fingerprints) on the skin and attach firmly to the skin

without detachment after repeated deformations. We found that the conformal and sticky structure of the stretchable METT can enable the crease amplification effect. The strain will focus on the crease of the skin, leading to the amplification of the output signal of the strain sensors on the METT. Besides, the METT has excellent stretchability and repeatability, so that the large local deformation (~500% for the one-layered METT when bending the finger; section S1 and fig. S1) caused by the crease amplification effect will not cause the failure or degradation of the strain sensors and interconnects based on metal-polymer conductors (MPCs). We pushed the limit of the thickness of the liquid metal-based electronic tattoo, making the METT multilayered and conformal simultaneously. Thus, any number of strain sensors or other functional components can be integrated, while the crease amplification effect can be retained, which is impossible to achieve with other techniques (25–33). On the basis of the METT, we can fabricate tattoos integrating 15 strain sensors and 1 heater, which is impossible for a single-layered electronic tattoo. We use the METT to heat the hand, monitor at most 15 degrees of freedom of the hand, and control a robotic hand remotely.

RESULTS AND DISCUSSION

Figure 1A presents the structure of a three-layered METT containing 1 heater and 15 strain sensors. The METT has the same structure as the commercial temporary transfer tattoo. It usually consists of three parts: an adhesive layer, a release layer, and circuit modules between the two. The adhesive layer is a thin layer of acrylic pressure-sensitive adhesive (~8 μm). When pressure is applied, the adhesive layer allows the METT to form a tight and conformal attachment to the skin. The acrylic pressure-sensitive adhesives are nontoxic since they have been successfully applied on various medical tapes. The release layer is a silicone film that can achieve an easy detachment of the circuit modules from the release film. The circuit layer (~14 μm for each layer) is a thin poly(styrene-butadiene-styrene) (SBS) film with stretchable conductors embedded in it. The circuit module in the three-layered METT contains three circuit layers, with 11 strain sensors on the first circuit layer, 4 strain sensors on the second circuit layer, and 1 heater on the third circuit layer. We choose the MPC to fabricate the circuit module, including interconnects, strain sensors, and heaters in the METT because of

¹Department of Biomedical Engineering, Shenzhen Bay Laboratory, Southern University of Science and Technology, No 1088, Xueyuan Rd, Xili, Nanshan District, Shenzhen, Guangdong 518055, P. R. China. ²School of Biomedical Engineering, Capital Medical University, No.10 Xitoutiao, You An Men Wai, Beijing 100069, P. R. China. ³National Center for Nanoscience and Technology, University of Chinese Academy of Sciences, No. 11 Zhongguancun Beiyitiao, Beijing 100190, P. R. China.
*Corresponding author. Email: jiang@sustech.edu.cn

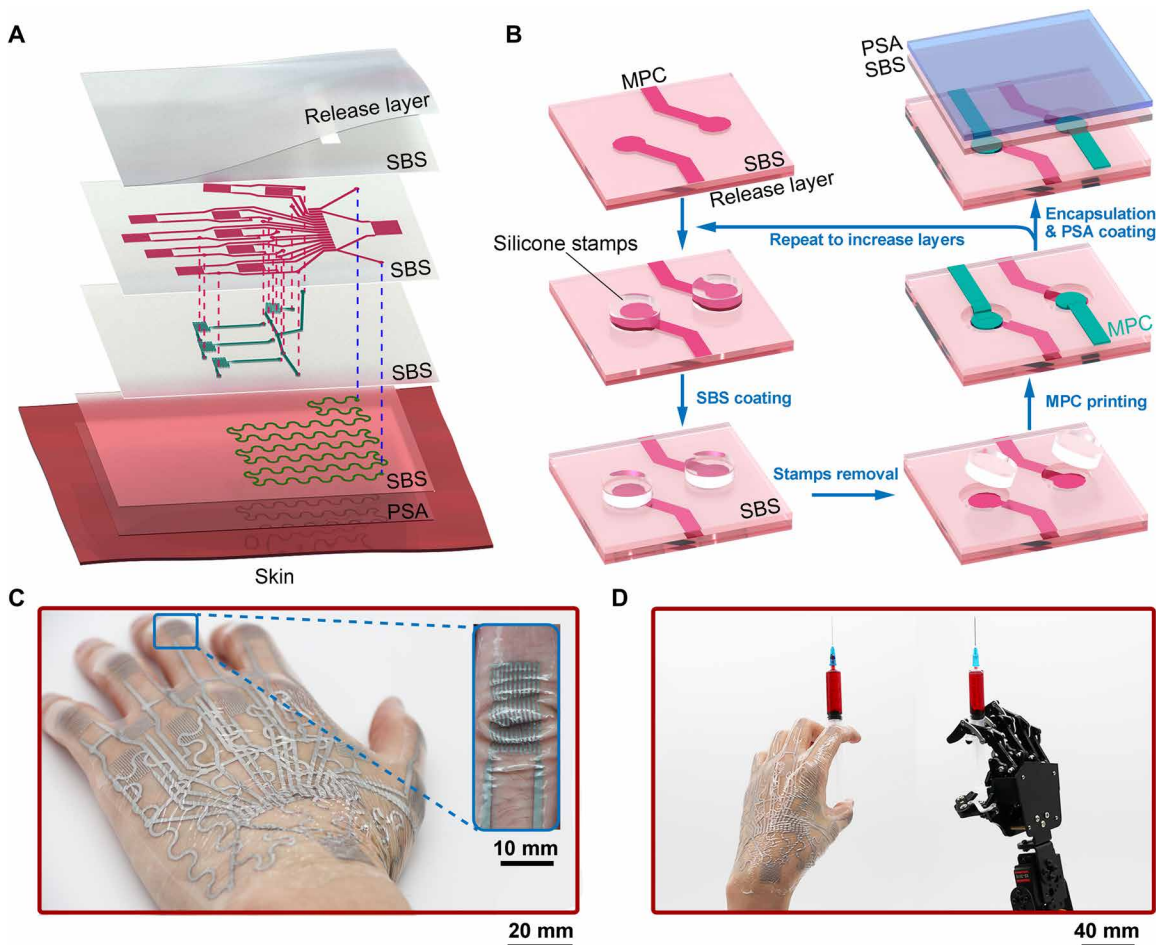


Fig. 1. Schematic illustrations and optical images of the three-layered METT. (A) Exploded schematics of the METT containing three circuit layers. (B) Schematic illustrations of the layer-by-layer fabrication of the METT. (C) Optical image of the METT after transferring onto the skin; inset, the METT can be embedded into the creases on the finger joints. (D) Optical image of the METT for remotely controlling a robotic hand. Photo credit: Lixue Tang, Southern University of Science and Technology.

the excellent conductivity and stretchability of the MPC. The purpose of the SBS film is to support the conductors and electrically isolate conductors in different layers. There are electric connection points (holes) on the SBS films for connecting conductors in different layers; thus, conductors in different layers will have vertical electric connections. When we attach the METT to the skin by pressure and remove the release layer, the circuit modules in the METT will be transferred onto the skin and form a firm attachment to the skin.

We created a layer-by-layer fabrication strategy to fabricate the METT. The fabrication (movie S1) starts from the outermost layer of the tattoo on the skin. We obtained a thin layer of notched SBS film on the release layer by spin-coating. The thickness of the SBS is spin-coating dependent (from 3 to 30 μm ; fig. S2). The MPC-based conductors can be directly printed onto the SBS film (Fig. 1B). If we continue to spin-coat another SBS film, the MPC will be completely sealed by the SBS film, losing electric connection with MPC in other layers. Thus, before the SBS coating, we placed the silicone stamps on electric connection points of the MPC, so that SBS will not seal MPC on those points during the SBS coating. After removing the silicone stamp, MPC on those points can provide vertical electric connections with other layers. We print MPC-based conductors on the second SBS film; MPC on the electric connection points will

form electrical connections with the MPC-based conductors on the bottom layer. We can increase the numbers of the circuit layers by repeating the procedures in Fig. 1B. Before the pressure-sensitive adhesive coating, we applied ~50% uniaxial strain on the METT to activate the circuit modules (make the MPC conductive). The MPC is not conductive after printing because of the nonconductive oxide layer on the liquid metal particles. When we stretch the METT, the stress will transmit from the substrate to the particles, breaking the oxide layer on the particles to generate conductive paths (32). The METT can attach firmly to the skin when pressure is applied, where no solvent or heat is needed to activate the adhesive. After removing the release layer, soft and thin circuit modules will remain on the skin (Fig. 1C). The three-layered METT can monitor 15 degrees of freedom of the hand, which suggests that the dexterity of the human hand can be transferred to the robotic hand if the robotic hand has enough degrees of freedom (Fig. 1D).

We tested the electro-mechanical performance of the MPC-based strain sensors in the METT. The MPC can be used as strain sensors because of the good stretchability and repeatability of the MPC. The resistance of the MPC-based strain sensors will increase with the increase of the tensile strain (Fig. 2, A and B). They can be easily stretched to a strain of 800% (Fig. 2A), which far exceeds the maximum

deformation of the skin. The MPC-based sensors in the METT also show excellent repeatability after being stretched to a strain of 50% for 1000 cycles (Fig. 2C). We measured the stress-strain curve of the METT, and we found that the METT with different layers has a similar strain-stress curve when the strain is less than 100% (fig. S3A). The METT modulus is 345 ± 16 kPa at a 50% strain, which is close to the skin modulus.

The stretchable METT is conformal and sticky, which can cause the crease amplification effect. The METT can be embedded into the creases on the skin such as finger creases (Fig. 2D) and fingerprint (Fig. 2E) because it is thin and soft. The skin within creases will not be completely covered by the METT, leaving the bottom of the creases uncovered. METT will bridge the two sides of the crease (Fig. 2, H and I). We call the METT on the bridge the “suspended part.”

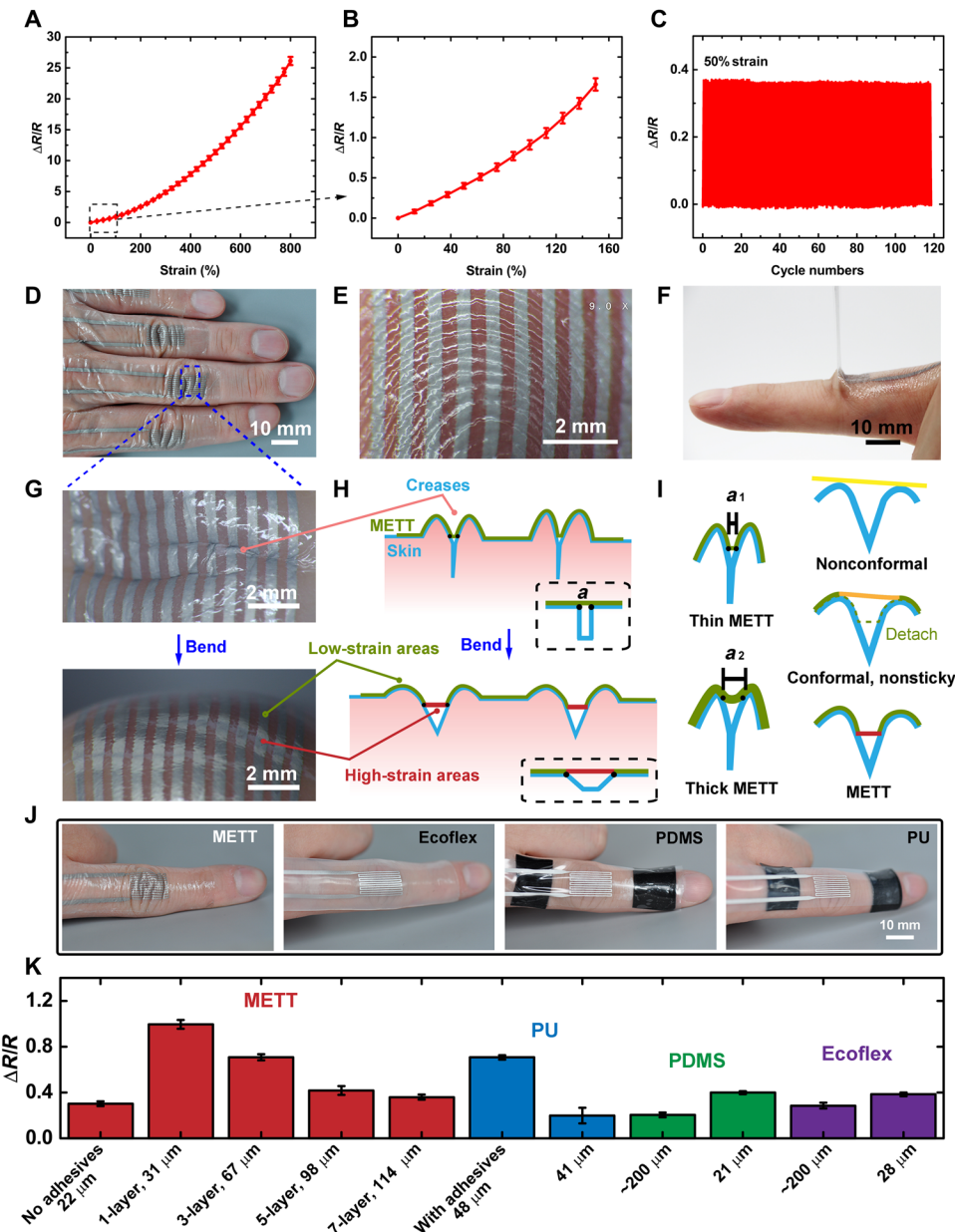


Fig. 2. The METT is conformal and sticky, which can enable the crease amplification effect. (A) $\Delta R/R$ of the MPC in METT versus different tensile strains from 0 to 800%. Error bars in this paper represent SE. (B) $\Delta R/R$ of the MPC in METT versus tensile strains from 0 to 150%. (C) Real-time monitoring of the strain sensor in METT by stretching the METT from a strain of 0 to 50% for about 100 cycles. (D) Photograph of the METT embedded in the creases of fingers. (E) The METT can be embedded in the fingerprint. (F) Photograph of peeling off the METT from the skin. (G) Enlarged view of the METT attaching to the proximal interphalangeal joints (PIPs) during bending. (H) Schematic illustrations of the crease amplification effect; “ a ” presents the initial length of the suspended part. Dashed box, the crease model. (I) Schematic illustrations of different substrates with different thicknesses on the crease. The initial length of the suspended part, $a_1 < a_2$. Strain when bending, red > orange > yellow. (J) Photographs of the strain sensors on the skin of finger joints with reference. (K) A comparison of the output signals of the MPC strain sensors on different substrates with different thicknesses when bending the index finger to 105°. Photo credit: Lixue Tang, Southern University of Science and Technology.

The length of the suspended part is METT thickness dependent (~ 0.2 mm for the one-layered METT; section S1). A thinner METT will lead to a deeper embedding of the crease, which will lead to a smaller initial length of the suspended part ($a_1 < a_2$, a_1 and a_2 present the initial length of the suspended part; Fig. 2I, left). Compared with the reported conformal electronic tattoo, the METT can attach firmly to the skin (Fig. 2F) within creases, which can ensure that strains will focus on those suspended parts when bending the fingers (Fig. 2G; the MPC on the creases is more reflective than the other parts; we believe that liquid metal particles within the METT under larger strain will be squeezed and have a flatter surface, thus appearing more reflective). As a result, the focused strain on the strain sensors will notably amplify the resistance compared with strain sensors under an average strain. We call this observation the crease amplification effect. According to the simulation and calculation from the crease model (section S1), we obtained the equation of the crease amplification effect, which can be written as

$$\frac{R' - R}{R} = \epsilon^2 \left(\frac{1}{an} - 1 \right)$$

in which R' is the resistance of the strain sensor under the crease amplification effect, R is the resistance of the strain sensor under average deformation, ϵ is the average strain of the strain sensors, a is the length of the suspended part, and n is the density of the creases. From the formula, we know that compared with the strain sensors under average deformation, the crease amplification effect can greatly amplify the output resistance if the product of a and n is much less than 1.

We fabricate METT with different layers to see how the thickness affects the output signals of strain sensors. In Fig. 2K, the deformation will be evenly loaded on the entire substrate during bending (Fig. 2I, right, nonconformal) when using the polydimethylsiloxane (PDMS; 200 μm) and Ecoflex (200 μm) as substrates, because such substrates are nonconformal, leading to small changes in the resistance of the strain sensors. By contrast, the METT can greatly increase the resistance of the strain sensors due to the crease amplification effect. We found that with the increase in the METT thickness, the crease amplification effect will decrease. That is because increasing the thickness of the METT will decrease the embedding depth of the METT, causing the increase in the initial length (a) of the suspended part. Besides, METT with a larger thickness requires a larger force to stretch to the same strain (fig. S3B). The METT will detach from the skin if the force exceeds the adhesion limit of the adhesives, which is equivalent to increasing the suspended part (a). According to the equation of the crease amplification effect, we know that the increase in the length of the suspended part (a) will decrease the crease amplification effect.

The pressure-sensitive adhesives are indispensable to the crease amplification effect. In Fig. 2K, the METTs without adhesive (22 μm), PDMS (21 μm), and Ecoflex (28 μm) are conformal; they can be embedded into the creases of fingers when used as substrates of strain sensors. When bending the finger, those substrates will detach from the skin (Fig. 2I, right, conformal but nonsticky), which is equivalent to increasing the initial length of the suspended part. By contrast, the METT can firmly attach to the skin even in deformation because of the pressure-sensitive adhesive, focusing the strain on the suspended part (Fig. 2I, right, METT). We can use PU (polyurethane) to fabricate the METT with the crease amplification effect (Fig. 2K). However, we cannot achieve a METT with the crease amplification

effect using silicones such as PDMS and Ecoflex. Those silicones have an inert surface and cannot attach to pressure-sensitive adhesives and, thus, cannot immobilize to the surface of fingers.

The pressure-sensitive adhesives can firmly attach the METT to the skin even during vigorous exercise. Figure 2F shows the removal of the METT from the proximal interphalangeal joint (PIP), which indicates that the pressure-sensitive adhesives can make the METT adhere to the skin firmly. The peel strength between the METT and the skin is 0.82 N cm^{-1} , which is much stronger than Ecoflex, PU, and PDMS (<0.01 N cm^{-1}). External supports are needed to fix the PDMS-based and PU-based strain sensors on PIP (Fig. 2J) when bending the finger. The Ecoflex-based sensors will detach from the finger when bending the finger (frequency = 2 Hz) while the sensor is facing the ground, because the gravity of the sensor is larger than the adhesion between the finger and the sensor. By contrast, the METT can attach firmly to the PIP without detachment even during vigorous exercise (bending the finger with a frequency of 4 Hz) while the sensor is facing the ground.

To demonstrate the scalability of the METT, we fabricate a seven-layered METT as a stretchable heater. Figure 3A presents the top view of the seven-layered heater. Each electric circuit layer contains one MPC-based serpentine heater with two connection points at both ends (Fig. 3A, top). Such electric connection points serve to form vertical electric connections with heaters in other layers (fig. S4). Thus, seven heaters on seven different layers are connected in series to the power supply. The thermal image (Fig. 3B) demonstrates that the MPC-based heaters in different layers have formed electric connections through the connection points. MPC in different layers other than the connection points has formed good electric insulations by the SBS, with no short circuits found in the thermal image. We applied 30% uniaxial strain to the seven-layered stretchable heater; the thermal image shows that this stretchable device still functions in deformations. However, with the increase in the number of layers, the conformability of the tattoo will decrease because of the increase of the thickness. Electronic tattoos with two layers are enough for most functions.

To balance the conformability and electric insulation between different METT layers, we need to determine the minimum thickness of the SBS. The METT needs to be very thin to become crease conformal. However, if the SBS layers for insulation are too thin, MPC-based conductors on different layers will lose electric isolations, causing a short circuit. We found that when the thickness is less than 13.70 μm , the SBS film has poor insulation capacity. From the scanning electron microscopy (SEM) characterization, we can see the outline of the MPC after coating the SBS film (4.8 μm) on the MPC (fig. S5). After stretching the MPC to a strain of 50% for 100 cycles, some of the liquid metal droplets will erupt from the SBS film (Fig. 3, C and D, left, and fig. S5A), causing a short circuit between different layers. When the SBS film thickness is 13.70 μm , there are no eruptions of liquid metals on the SBS film, whether at rest or in deformation (Fig. 3, C and D, right, and fig. S5B). The conductivity test of MPC on different layers also shows good insulation. To obtain METT with good conformability and isolation capacity, we need to fabricate SBS layers with a thickness close to 14 μm .

The n -layered METT usually contains an $n + 1$ SBS layer. To ensure good electric insulation and conformability, the thickness of each SBS layer should be about 14 μm . As a result, the circuit modules transferred onto the skin will have a thickness of $14n + 22$ μm . The one-layered METT can be embedded in fingerprints. However,

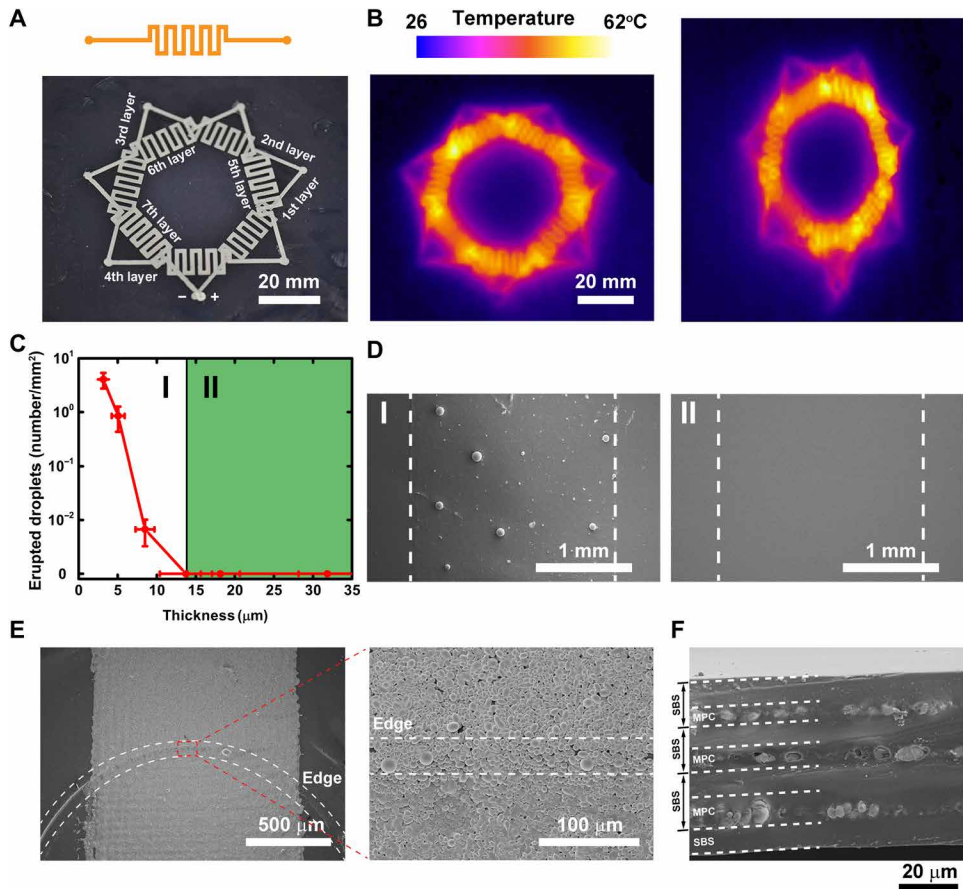


Fig. 3. The scalability of the METT. (A) Optical image of the seven-layered heater. (B) The thermal image of the heater without deformation (left) and with 30% strain (right). (C) The numbers of the erupted liquid metal droplets depend on the thickness of the SBS layer after the stretch cycles. (D) Scanning electron microscopy (SEM) characterization of the surface of the SBS corresponding to (C); the thickness of the SBS in I (left) and II (right) is 4.8 and 18.13 μm , respectively. (E) SEM characterizations of the electric connection point. The dotted lines present the edge of the electric connection point, which is covered by liquid metal particles. (F) Cross section of a three-layered METT.

the increase in the number of circuit layers will sacrifice the conformability of the METT. The three-layered METT will lose its conformability on fingerprint, but it can still be embedded into the creases on PIP. We usually fabricate METT with two circuit layers that can meet most conditions of circuit design.

We studied the electric connection points for connecting MPC on different layers. In Fig. 1B, when the silicone stamp is removed, a shallow blind hole will be left on the SBS film, the MPC on those points will be exposed, while other parts will be sealed by the SBS. Those blind holes are called electric connection points. After we print another layer of MPC on the SBS film, MPC on different layers will form vertical connections on the electric connection points. The depth of the hole equals the thickness of the SBS film. We found that the edge of the blind holes with a depth of 13.70 μm will not block the MPC paths. From the SEM characterization, we can see that liquid metal particles can fill the edges of the blind holes, connecting MPC on different SBS layers (Fig. 3E). However, when we increase the depth of the blind hole to about 18.13 μm , from the SEM characterization, the MPC paths will be blocked by the edge of the holes (fig. S6A). To rebuild the MPC paths, we usually add a drop of MPC ink (50 μl) to the edge of the holes (fig. S6B). Thus, we can fabricate multilayered circuit modules through the electric connection points.

We characterized the cross section of a three-layered METT. From the SEM characterization (Fig. 3F), we found that the cross section presents a three-layered structure. Discontinuous liquid metal particles are embedded in the SBS film, which suggests that liquid metal particles have formed conductive networks in each layer. The SBS has formed good insulation between the MPC layers.

We use the METT to measure the motions of the hand. We use the one-layered METT to measure the bending angle of the PIP (angle α), metacarpophalangeal joints (MCPs; angle β), wrist, and the opening angle of two adjacent fingers (OAFs; angle γ), respectively. The position of the sensors on the hand is shown in Fig. 4D. The results (Fig. 4A and fig. S7) show that sensors attached to the PIPs (sensitivity $\approx 0.93 \text{ ohms}^{-1}$, $R_0 = 120 \text{ ohms}$) have larger sensitivity than those on MCPs (sensitivity $\approx 0.23 \text{ ohms}^{-1}$, $R_0 = 120 \text{ ohms}$) and wrist (sensitivity $\approx 0.50 \text{ ohms}^{-1}$, $R_0 = 140 \text{ ohms}$). From the equation of the crease amplification effect, we know that the smaller initial length of the suspended part and the smaller density of the creases on skin lead to the larger output resistance of the strain sensor. We believe that the initial length of the suspended part is METT thickness dependent. Thus, the METTs on the PIPs and MCPs have the same initial length of the suspended part. However, the MCPs ($\sim 1.3 \text{ mm}^{-1}$) have a larger density of creases than the PIPs ($\sim 0.4 \text{ mm}^{-1}$) (fig. S8). Thus, output signals of strain sensors on the PIPs are larger than

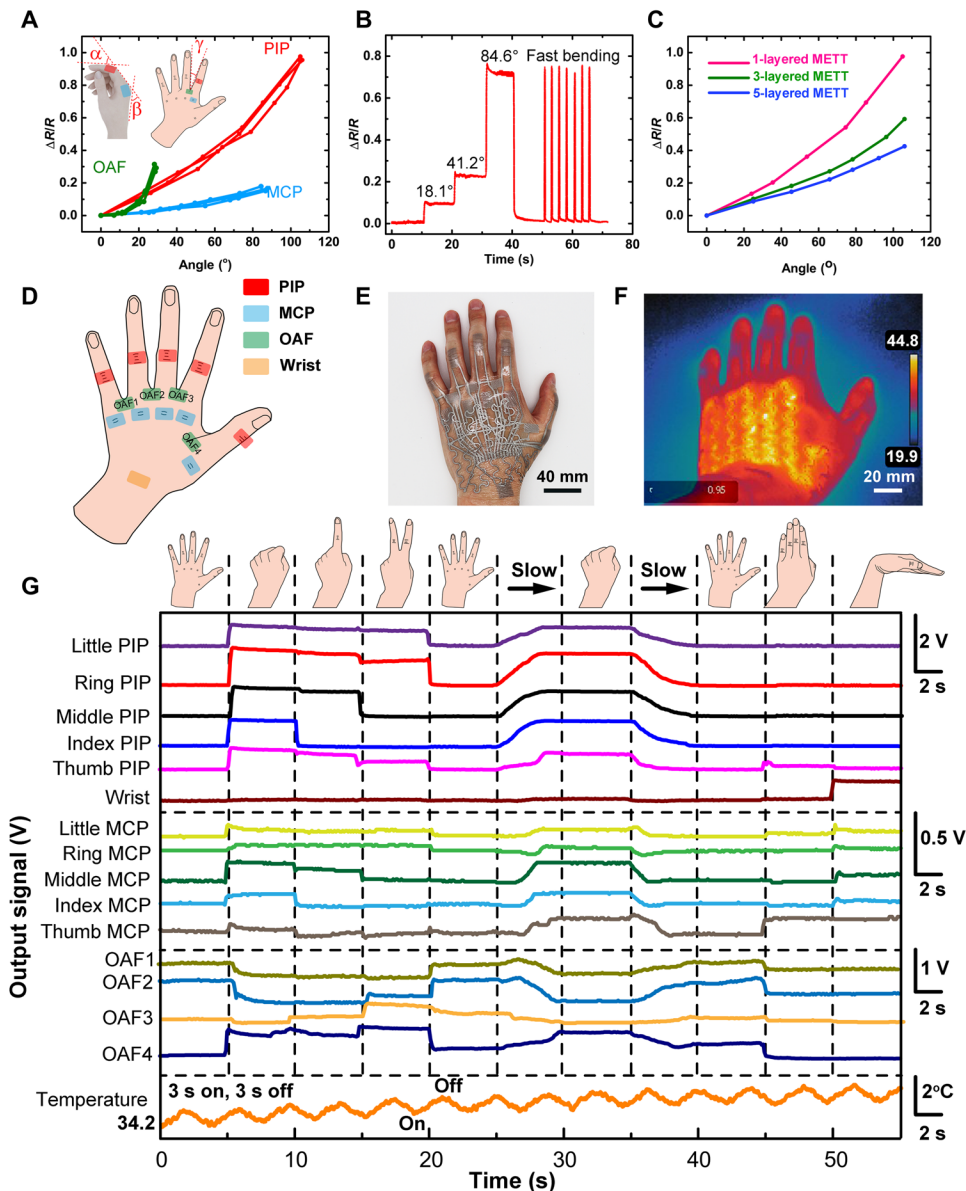


Fig. 4. The METT can monitor the movements of the hand. (A) $\Delta R/R$ of strain sensors in different position versus angles. Inset: The schematic illustration of the measurement positions of the strain sensors. (B) Resistance response of the METT attached to PIP in different bending angles. (C) $\Delta R/R$ of strain sensors in the METT with different layers depending on the bending angles of the index PIP. (D) Schematic illustration of the measurement positions of the strain sensors. (E) Optical images of the three-layered METT attaching to the hand. (F) The thermal image of the three-layered METT on hand. (G) The real-time signal changes of the 15 strain sensors and temperature changes of the heater on the METT with different hand movements. Photo credit: Lixue Tang, Southern University of Science and Technology.

those on the MCPs when bending to the same angle. We also use the METT to measure the OAFs. We found that sensors have low sensitivity at angles less than 20° (sensitivity $\approx 0.11 \text{ ohms}/^{\circ}$, $R_0 = 90 \text{ ohms}$), because strain sensors are not in a stretched state before reaching 20°. However, when the open angle is larger than 20°, the resistance of the sensors increases sharply (sensitivity $\approx 2.01 \text{ ohms}/^{\circ}$, $R_0 = 90 \text{ ohms}$) because the gap between two fingers can be regarded as one crease. When we splay/spread the fingers, all the deformations will focus on the METT above the only crease, which will greatly increase the sensitivity of the strain sensors. However, the pressure-sensitive adhesives for attaching the METT to the skin have limited adhesive strength (about 0.82 N cm^{-1}). When the stress caused by the large

strain exceeds the adhesion limit of the adhesives, the METT around the crease will detach from the skin (fig. S9), causing a decrease in the output signals. Thus, the METT can qualitatively measure the opening angles. To solve the problem of detachment, on the one hand, we can adopt pressure-sensitive adhesives with larger adhesive strength to fabricate the METT. On the other hand, we can use stretchable materials with smaller modulus and thickness to fabricate the METT. Figure 4B shows the performance of the strain sensor on PIP for real-time movement monitoring of the index finger; we found that each strain of the strain sensor corresponds to a resistance value. The strain sensor shows excellent repeatability when bending the finger with high frequency.

We attach the three-layered METT in Fig. 1 containing 15 strain sensors (Fig. 4D) and 1 heater to the left hand to test its performances in strain sensing and heating (Fig. 4E). Using the three-layered METT, we can simultaneously measure the movement of the hand in 15 degrees of freedom and adjust the temperature, which is impossible for reported single-layered electronic tattoos. Figure 4F shows the heating performance of the heater; the MPC heater in the METT can heat the back of the hand to a temperature of about 45°C in 30 s. The serpentine shape of the heater in the thermal image also demonstrates that the SBS layer can form good insulation between different circuit layers since no short circuit is found. Although the increase in the METT layers will decrease the sensitivity of the strain sensors on the METT (Fig. 4C), the three-layered METT is capable of monitoring the motions of the hand. Figure 4G shows the real-time signal changes of the 15 strain sensors and temperature changes of the heater on the METT with different hand movements. We can adjust the temperature of the heater on the METT by controlling the on-off time. The temperature will gradually increase from 34° to 37°C in about 1 min (3 s on and 3 s off). We found that the measurement of the PIP is very sensitive. The output signals on PIP are about three to four times that of MCP and OAF. Small-angle changes on the PIP can cause obvious signal changes. For example, the signal change of the ring PIP can be easily recognized from gesture “1” to gesture “2” at the 15th second. By contrast, the measurement of MCP and OAF is not sensitive at small angles. Angles imposed on the MCP and OAF must exceed a certain value to be recognized when slowly extending the hand from the full extension of the fingers to a fist (25 to 30 s). In general, we can use METT to measure hand movements.

We achieved a two-layer METT to remotely control a robotic hand with 6 degrees of freedom. This two-layer METT contains five strain sensors on PIPs and one strain sensor on the wrist, which can monitor 6 degrees of freedom in real time. The METT can be directly

transferred onto the hand or a disposable glove by attaching it to the surface and removing the release film (Fig. 5, A and B). The METT can be transferred to most substrates only if the pressure-sensitive adhesives in the METT are sticky to the substrates. The METT is controlled by a watch-like device through the external contact pads (Fig. 5B). Figure 5C shows the system-level overview of the robot control system, which contains signal transduction, conditioning, processing, and transmission paths. The circuit design for the sensing system is shown in fig. S10. The strain sensors are connected to Wheatstone bridges. Signals caused by bending the fingers will be amplified and transmitted to the robotic hand through Bluetooth. As a result, we can wear the METT to control the robotic hand wirelessly. The robotic hand can imitate the movements of our hand without abnormal vibration (Fig. 5D and movie S2). The signals obtained from the METT attached to the PIP when we make various gestures are shown in Fig. 4G, which suggests that strain sensors on fingers have good repeatability and do not interfere with each other. Signals from each finger are stable when the finger remains stationary, which avoids the abnormal vibration of the robotic hand. This robot control system will have great potential in the medical system and military field for performing dangerous tasks remotely.

Conclusions

In this work, we have achieved multilayered electronic tattoos that can enable the crease amplification effect. We found that the conformal and sticky structure of the stretchable METT can enable the crease amplification effect, which will lead to the amplification of the output signal of the strain sensors on the METT. We create a layer-by-layer fabrication strategy to fabricate the METT with different layers, while the crease amplification effect can be retained.

The MPC is indispensable in the METT, because the MPC-based strain sensors and interconnects have excellent stretchability and repeatability, which can function in large local deformation (~500%

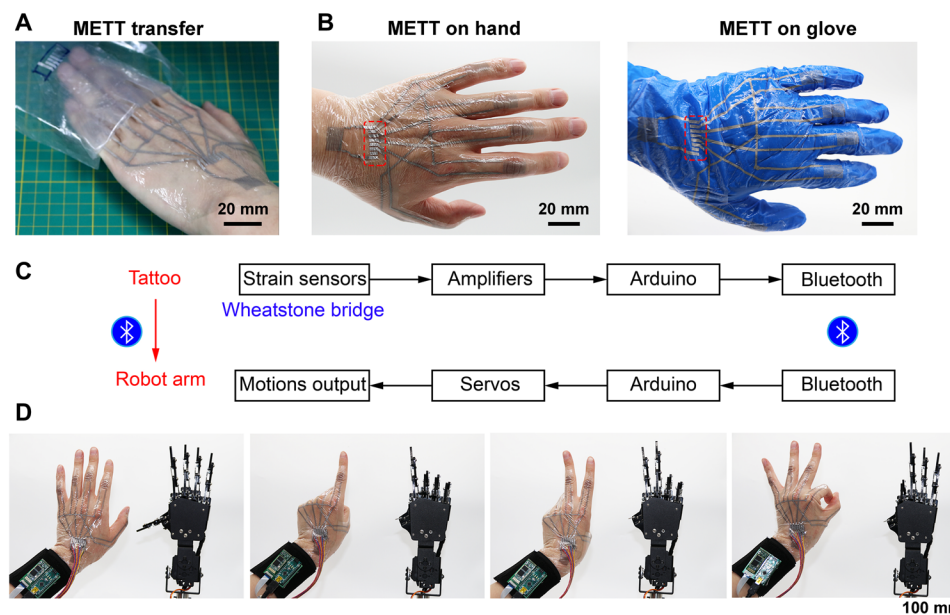


Fig. 5. The METT can control the robotic hand remotely. (A) Photograph of transferring the tattoo onto the hand. (B) Photograph showing METT on the skin (left) and disposal glove (right). Dotted frame, the external contact pads. (C) System-level block diagram of the robot controlling system. (D) The METT can remotely control the movements of the robotic hand. Photo credit: Lixue Tang, Southern University of Science and Technology.

for the one-layered METT on the PIP when bending the finger; section S1) caused by the crease amplification effect.

By contrast, the carbon nanomaterials such as graphene and carbon nanotubes usually have poor conductivity (0.1 to 100 S/m) and low stretchability (<200%) (34, 35). They have potentials as strain sensors, but they are not suitable as stretchable interconnects because their conductivity is several orders of magnitude worse than that of metal. Besides, the large local deformation (~500%) caused by the crease amplification effect will cause the failure of the carbon nanomaterial-based strain sensors.

The nanostructured metal, especially the silver nanowires, has comparable conductivity and satisfactory stretchability (~800%). They have the potential as stretchable interconnects, but they are not suitable as strain sensors because the repeatability of the nanostructured metal is poor. The electrical performance of the silver nanowire will degrade slowly or sharply with the deformation cycles (36, 37). Besides, the electrical performance of the silver nanowire will decrease because of the high oxidation tendency of Ag.

Using the three-layered METT, we can measure 15 degrees of freedom of the hand. We believe that by increasing the degrees of freedom in robotic hands, we can use the robotic control system to perform delicate and complicated tasks remotely, which have a great potential in the medical system, virtual reality, and wearable robots. In the future, we can fabricate creases/cracks on the MPC-based strain sensors, and the sensitivity of the MPC-based strain sensors can be adjusted by the density and the width of the creases/cracks. Thus, the strain sensors based on the crease amplification effect will have broader applications, not limited to skin with creases.

MATERIALS AND METHODS

Solution preparation

We added 30 g of SBS [30 weight %; average M_w (weight-average molecular weight) ~140,000; Sigma-Aldrich, USA] into 170 g of di(propylene glycol) methyl ether acetate and stirred for 24 hours at a temperature of 60°C to obtain the SBS solution. We added 1 g of PVP [polyvinyl pyrrolidone; M_n (number-average molecular weight) = 1,300,000, Aladdin, China] into 19 g of hexyl alcohol (98%, Macklin, China) and stirred for 48 hours to obtain the PVP solution. We sonicated 3 g of liquid metal (gallium-indium alloy; Ga:In = 4:1, Hawk, HK3284, China) in 1 ml of PVP solution to obtain the MPC ink. The sonication process was carried out for 60 s using a probe sonicator (S450D, Branson, USA) at an amplitude of 20% (5 s on and 10 s off).

Fabrication of the METT

The layer-by-layer fabrication of the METT started by choosing the release film. We chose the silicone membrane as the release film (0.2 mm, shengyujin, China) since the SBS film can be easily detached from the silicone membrane. We stuck the Scotch tape on the release film where external contacts (Fig. 5B) are supposed to be exposed after the transfer of the METT. We spin-coated (KW-4A, SETCAS, China) the SBS solution on the silicone membrane at 800 rpm for 20 s. The Scotch tape should be removed before the evaporation of the SBS solvent. We cured the SBS film on an 80°C oven (DHG-9420A, Yiheng Scientific Instrument Co. Ltd., China) for 10 min. We screen-printed the MPC ink on the SBS film and allowed it to dry in an 80°C oven for 2 min. Before the coating of the second-layer SBS, we placed the silicone stamps on the electric connection points

of the MPC to prevent the sealing of those points by SBS. We repeated the spin-coating process and removed the silicone stamps before the evaporation of the SBS solvent. After the curing of the second-layer SBS, we printed another layer of MPC after alignment. As a result, we can obtain METT with desirable MPC layers by repeating the process above. We used the water-based acrylic pressure-sensitive adhesives (808, Wending Sticky Treasure, China) to fabricate the pressure-sensitive adhesive layer in the METT. After evaporation of the water, acrylic monomers were polymerized to produce an acrylic pressure-sensitive polymer. To prove that the acrylic pressure-sensitive adhesives are nontoxic, we attached the one-layered METT (width, 2 cm; length, 2 cm) to the skin of the forearm for 24 hours. No itchiness, irritation, or other feelings of discomfort were found. Besides, acrylic pressure-sensitive adhesives have been successfully applied on various medical tapes. Before the spin-coating of the pressure-sensitive adhesive, we applied a 50% unidirectional tensile strain on the METT and then applied another 50% unidirectional tensile strain to the vertical direction to make the MPC conductive. We spin-coated a layer of pressure-sensitive adhesive on the SBS layer at 2000 rpm for 20 s and allowed it to cure in an 80°C oven for 10 min. After attaching the METT to the skin or other surfaces, we can remove the release film; thus, the MPC circuit modules can be transferred on the skin or other surfaces.

Characterization of the METT

To fabricate samples for SBS film characterization, we placed silicone stamps on an MPC printed SBS film and spin-coated SBS solutions in different speeds and for different times (3000 rpm, 1500 rpm, 800 rpm, 1500 rpm two times, and 800 rpm two times) to obtain SBS layers with different thicknesses (fig. S2). Spin-coating SBS solution for two times means that we spin-coated SBS solution on the MPC-printed SBS film. After its curing, we spin-coated another SBS at the same speed. After the removal of the silicone stamp, we used a stylus profiler (Bruker, DektakXT, USA) to measure the thickness of the SBS films. We applied 50% unidirectional tensile strain on samples for 100 cycles. After the tensile cycles, we used a scanning electron microscope (Hitachi, S8220, Japan) to characterize the surface of the SBS film to see if there are liquid metal eruptions. The peel strength between the METT and the skin is measured by the 180° peel method using the universal testing machines (3365, Instron, USA).

We transferred the METT onto the stretchable 3M VHB tape and carried out a mechanical test to the METT attached 3M VHB substrate. We used a linear guide slide (FSL_40, FUYU, China) to apply tensile strains on samples and used an electrochemical station (1040C, CHI, China) (technique, the amperometric $i-t$ curve at a potential of 0.001 V) to record the electrical signals of the samples under deformations. The electrochemical station carries out the individual test of strain sensors on different substrates.

The circuit design of the signal processing module is shown in fig. S10. The circuit module contains six Wheatstone bridges and six instrumental amplifiers (AD627) for amplifying signals from the strain sensors in the METT. The 15 strain sensors in the three-layered METT are connected to three signal processing modules. The 15 strain sensors are controlled by Arduino Mega 2560. The heater is powered by a source meter (2601B, Keithley, USA) in a current of 0.12 A and controlled by Arduino Mega 2560 through a relay. The temperature of the heater is tested by a heat gun (E40, FLIR, USA) and monitored by LM35 that is directly attached to the heater.

The robot controlling system contains a signal processing module for amplifying the signals from the two-layered METT, a Bluetooth module (HC-05) for sending the signals to the controller (Arduino Uno) of the robotic hand, and a controller (Arduino Nano). The robotic hand (uHand2.0, Shanghai Langyi Electronic Technology Co. Ltd., China) is controlled by Arduino Uno connected by a Bluetooth module (HC-05). The METTs are tested in the hand of authors and approved by the institutional ethics committee (SUSTech Institutional Review Board, 20200085).

SUPPLEMENTARY MATERIALS

Supplementary material for this article is available at <http://advances.sciencemag.org/cgi/content/full/7/3/eabe3778/DC1>

REFERENCES AND NOTES

- Lee, D., Sasaki, D., Kim, M., Mori, T., Yokota, H., Lee, S., Park, K., Fukuda, M., Sekino, K., Matsura, T., Shimizu, T., Someya, T., Ultrasoft electronics to monitor dynamically pulsing cardiomyocytes. *Nat. Nanotechnol.* **14**, 156–160 (2019).
- R. M. Torrente-Rodríguez, J. Tu, Y. Yang, J. Min, M. Wang, Y. Song, Y. Yu, C. Xu, C. Ye, W. W. IshHak, W. Gao, Investigation of cortisol dynamics in human sweat using a graphene-based wireless mhealth system. *Mater. Matter* **2**, 921–937 (2020).
- J. T. Reeder, J. Choi, Y. Xue, P. Gutruf, J. Hanson, M. Liu, T. Ray, A. J. Bandodkar, R. Avila, W. Xia, S. Krishnan, S. Xu, K. Barnes, M. Pahnke, R. Ghaffari, Y. Huang, J. A. Rogers, Waterproof, electronics-enabled, epidermal microfluidic devices for sweat collection, biomarker analysis, and thermography in aquatic settings. *Sci. Adv.* **5**, eaau6356 (2019).
- H. U. Chung, A. Y. Rwei, A. Hourlier-Fargette, S. Xu, K. H. Lee, E. C. Dunne, Z. Xie, C. Liu, A. Carlini, D. H. Kim, D. Ryu, E. Kulikova, J. Cao, I. C. Odland, K. B. Fields, B. Hopkins, A. Banks, C. Ogle, D. Grande, J. B. Park, J. Kim, M. Irie, H. Jang, J. H. Lee, Y. Park, J. Kim, H. H. Jo, H. Hahm, R. Avila, Y. Xu, M. Namkoong, J. W. Kwak, E. Suen, M. A. Paulus, R. J. Kim, B. V. Parsons, K. A. Human, S. S. Kim, M. Patel, W. Reuther, H. S. Kim, S. H. Lee, J. D. Leedle, Y. Yun, S. Rigali, T. Son, I. Jung, H. Arafa, V. R. Soundararajan, A. Ollech, A. Shukla, A. Bradley, M. Schau, C. M. Rand, L. E. Marsillio, Z. L. Harris, Y. Huang, A. Hamvas, A. S. Paller, D. E. Weese-Mayer, J. Y. Lee, J. A. Rogers, Skin-interfaced biosensors for advanced wireless physiological monitoring in neonatal and pediatric intensive-care units. *Nat. Med.* **26**, 418–429 (2020).
- H. Lee, C. Song, Y. S. Hong, M. S. Kim, H. R. Cho, T. Kang, K. Shin, S. H. Choi, T. Hyeon, D.-H. Kim, Wearable/disposable sweat-based glucose monitoring device with multistage transdermal drug delivery module. *Sci. Adv.* **3**, e1601314 (2017).
- Y. Ling, T. An, L. W. Yap, B. Zhu, S. Gong, W. Cheng, Disruptive, soft, wearable sensors. *Adv. Mater.* **32**, 1904664 (2019).
- R. Dong, Y. Liu, L. Mou, J. Deng, X. Jiang, Microfluidics-based biomaterials and biodevices. *Adv. Mater.* **31**, 1805033 (2019).
- J. Lee, H. R. Cho, G. D. Cha, H. Seo, S. Lee, C.-K. Park, J. W. Kim, S. Qiao, L. Wang, D. Kang, T. Kang, T. Ichikawa, J. Kim, H. Lee, W. Lee, S. Kim, S.-T. Lee, N. Lu, T. Hyeon, S. H. Choi, D.-H. Kim, Flexible, sticky, and biodegradable wireless device for drug delivery to brain tumors. *Nat. Commun.* **10**, 5205 (2019).
- S. Park, S. W. Heo, W. Lee, D. Inoue, Z. Jiang, K. Yu, H. Jinno, D. Hashizume, M. Sekino, T. Yokota, K. Fukuda, K. Tajima, T. Someya, Self-powered ultra-flexible electronics via nano-grating-patterned organic photovoltaics. *Nature* **561**, 516–521 (2018).
- Q. Huang, D. Wang, H. Hu, J. Shang, J. Chang, C. Xie, Y. Yang, X. Lepró, R. H. Baughman, Z. Zheng, Additive functionalization and embroidery for manufacturing wearable and washable textile supercapacitors. *Adv. Funct. Mater.* **30**, 1910541 (2020).
- L. Wang, L. Wang, Y. Zhang, J. Pan, S. Li, X. Sun, B. Zhang, H. Peng, Weaving sensing fibers into electrochemical fabric for real-time health monitoring. *Adv. Funct. Mater.* **28**, 1804456 (2018).
- S. Choi, S. I. Han, D. Jung, H. J. Hwang, C. Lim, S. Bae, O. K. Park, C. M. Tschaubrunn, M. Lee, S. Y. Bae, J. W. Yu, J. H. Ryu, S.-W. Lee, K. Park, P. M. Kang, W. B. Lee, R. Nezafat, T. Hyeon, D.-H. Kim, Highly conductive, stretchable and biocompatible Ag–Au core–sheath nanowire composite for wearable and implantable bioelectronics. *Nat. Nanotechnol.* **13**, 1048–1056 (2018).
- L. Tang, S. Cheng, L. Zhang, H. Mi, L. Mou, S. Yang, Z. Huang, X. Shi, X. Jiang, Printable metal-polymer conductors for highly stretchable bio-devices. *iScience* **4**, 302–311 (2018).
- T. Ha, J. Tran, S. Liu, H. Jang, H. Jeong, R. Mitbander, H. Huh, Y. Qiu, J. Duong, R. L. Wang, P. Wang, A. Tandon, J. Sirohi, N. Lu, A chest-laminated ultrathin and stretchable E-tattoo for the measurement of electrocardiogram, seismocardiogram, and cardiac time intervals. *Adv. Sci.* **6**, 1900290 (2019).
- Y. J. Hong, H. Jeong, K. W. Cho, N. Lu, D.-H. Kim, Wearable and implantable devices for cardiovascular healthcare: From monitoring to therapy based on flexible and stretchable electronics. *Adv. Funct. Mater.* **29**, 1808247 (2019).
- S. Xu, Y. Zhang, L. Jia, K. E. Mathewson, K.-I. Jang, J. Kim, H. Fu, X. Huang, P. Chava, R. Wang, S. Bhole, L. Wang, Y. J. Na, Y. Guan, M. Flavin, Z. Han, Y. Huang, J. A. Rogers, Soft microfluidic assemblies of sensors, circuits, and radios for the skin. *Science* **344**, 70–74 (2014).
- W. Gao, S. Emaminejad, H. Y. Y. Nyein, S. Challa, K. Chen, A. Peck, H. M. Fahad, H. Ota, H. Shiraki, D. Kiriyama, D.-H. Lien, G. A. Brooks, R. W. Davis, A. Javey, Fully integrated wearable sensor arrays for multiplexed *in situ* perspiration analysis. *Nature* **529**, 509–514 (2016).
- S. Gong, L. W. Yap, B. Zhu, Q. Zhai, Y. Liu, Q. Lyu, K. Wang, M. Yang, Y. Ling, D. T. H. Lai, F. Marzbanrad, W. Cheng, Local crack-programmed gold nanowire electronic skin tattoos for in-plane multisensor integration. *Adv. Mater.* **31**, 1903789 (2019).
- Z. Huang, Y. Hao, Y. Li, H. Hu, C. Wang, A. Nomoto, T. Pan, Y. Gu, Y. Chen, T. Zhang, W. Li, Y. Lei, N. H. Kim, C. Wang, L. Zhang, J. W. Ward, A. Maralani, X. Li, M. F. Durstock, A. Pisano, Y. Lin, S. Xu, Three-dimensional integrated stretchable electronics. *Nat. Electron.* **1**, 473–480 (2018).
- D. Green Marques, P. Alhais Lopes, A. T. de Almeida, C. Majidi, M. Tavakoli, Reliable interfaces for EGaN multi-layer stretchable circuits and microelectronics. *Lab Chip* **19**, 897–906 (2019).
- K. B. Oztemiz, J. Wissman, O. B. Ozdoganlar, C. Majidi, EGaN–metal interfacing for liquid metal circuitry and microelectronics integration. *Adv. Mater. Interfaces* **5**, 1701596 (2018).
- D.-H. Kim, N. Lu, R. Ma, Y.-S. Kim, R.-H. Kim, S. Wang, J. Wu, S. M. Won, H. Tao, A. Islam, K. J. Yu, T.-I. Kim, R. Chowdhury, M. Ying, L. Xu, M. Li, H.-J. Chung, H. Keum, M. M. Cormick, P. Liu, Y.-W. Zhang, F. G. Omenetto, Y. Huang, T. Coleman, J. A. Rogers, Epidermal electronics. *Science* **333**, 838–843 (2011).
- Y. R. Jeong, J. Kim, Z. Xie, Y. Xue, S. M. Won, G. Lee, S. W. Jin, S. Y. Hong, X. Feng, Y. Huang, J. A. Rogers, J. S. Ha, A skin-attachable, stretchable integrated system based on liquid gainsns for wireless human motion monitoring with multi-site sensing capabilities. *NPG Asia Mater.* **9**, e433 (2017).
- J. Shin, B. Jeong, J. Kim, V. B. Nam, Y. Yoon, J. Jung, S. Hong, H. Lee, H. Eom, J. Yeo, J. Choi, D. Lee, S. H. Ko, Sensitive wearable temperature sensor with seamless monolithic integration. *Adv. Mater.* **32**, 1905527 (2019).
- Z. Zhu, S.-Z. Guo, T. Hirdler, C. Eide, X. Fan, J. Tolar, M. C. McAlpine, 3D printed functional and biological materials on moving freeform surfaces. *Adv. Mater.* **30**, 1707495 (2018).
- R. Guo, B. Cui, X. Zhao, M. Duan, X. Sun, R. Zhao, L. Sheng, J. Liu, J. Lu, Cu–EGaN enabled stretchable e-skin for interactive electronics and CT assistant localization. *Mater. Horiz.* **7**, 1845–1853 (2020).
- Y. Yu, J. Zhang, J. Liu, Biomedical implementation of liquid metal ink as drawable ECG electrode and skin circuit. *PLOS ONE* **8**, e58771 (2013).
- C. Guo, Y. Yu, J. Liu, Rapidly patterning conductive components on skin substrates as physiological testing devices via liquid metal spraying and pre-designed mask. *J. Mater. Chem. B* **2**, 5739–5745 (2014).
- P. A. Lopes, H. Paisana, A. T. De Almeida, C. Majidi, M. Tavakoli, Hydroprinted electronics: Ultrathin stretchable Ag–In–Ga E-skin for bioelectronics and human-machine interaction. *ACS Appl. Mater. Interfaces* **10**, 38760–38768 (2018).
- L. Dejace, N. Laubeuf, I. Furfarò, S. P. Lacour, Gallium-based thin films for wearable human motion sensors. *Adv. Intell. Syst.* **1**, 1900079 (2019).
- L. Tang, L. Mou, J. Shang, J. Dou, W. Zhang, X. Jiang, Metal-hygroscopic polymer conductors that can secrete solders for connections in stretchable devices. *Mater. Horiz.* **7**, 1186–1194 (2020).
- L. Tang, L. Mou, W. Zhang, X. Jiang, Large-scale fabrication of highly elastic conductors on a broad range of surfaces. *ACS Appl. Mater. Interfaces* **11**, 7138–7147 (2019).
- J.-H. Ahn, H.-S. Kim, K. J. Lee, S. Jeon, S. J. Kang, Y. Sun, R. G. Nuzzo, J. A. Rogers, Heterogeneous three-dimensional electronics by use of printed semiconductor nanomaterials. *Science* **314**, 1754–1757 (2006).
- D. J. Lipomi, M. Vosgueritchian, B. C.-K. Tee, S. L. Hellstrom, J. A. Lee, C. H. Fox, Z. Bao, Skin-like pressure and strain sensors based on transparent elastic films of carbon nanotubes. *Nat. Nanotechnol.* **6**, 788–792 (2011).
- H. Jang, Y. J. Park, X. Chen, T. Das, M.-S. Kim, J.-H. Ahn, Graphene-based flexible and stretchable electronics. *Adv. Mater.* **28**, 4184–4202 (2016).
- S. Choi, J. Park, W. Hyun, J. Kim, J. Y. B. Lee, C. Song, H. J. Hwang, J. H. Kim, T. Hyeon, D.-H. Kim, Stretchable heater using ligand-exchanged silver nanowire nanocomposite for wearable articular thermotherapy. *ACS Nano* **9**, 6626–6633 (2015).
- N. Matsuhisa, D. Inoue, P. Zalar, H. Jin, Y. Matsuba, A. Itoh, T. Yokota, D. Hashizume, T. Someya, Printable elastic conductors by *in situ* formation of silver nanoparticles from silver flakes. *Nat. Mater.* **16**, 834–840 (2017).

Acknowledgments

Funding: We thank the National Key R&D Program of China (2018YFA0902600 and 2017YFA0205901), the National Natural Science Foundation of China (21535001, 81730051, and 21761142006), Shenzhen Bay Laboratory (SZBL2019062801004), the High-level University Construction Fund from Shenzhen Government (nos. G02386301 and G02386401), and the Tencent Foundation through the XPLORER PRIZE for financial support. **Author contributions:**

X.J. conceived and supervised this project. L.T. designed, fabricated, and characterized the METT. J.S. screened the polymers for fabricating the METT. L.T., J.S., and X.J. wrote the manuscript. All authors discussed the results and commented on the manuscript. **Competing interests:** The authors declare that they have no competing interests. **Data and materials availability:** All data needed to evaluate the conclusions in the paper are present in the paper and/or the Supplementary Materials. Additional data related to this paper may be requested from the authors.

Submitted 18 August 2020
Accepted 17 November 2020
Published 13 January 2021
10.1126/sciadv.abe3778

Citation: L. Tang, J. Shang, X. Jiang, Multilayered electronic transfer tattoo that can enable the crease amplification effect. *Sci. Adv.* **7**, eabe3778 (2021).

Science Advances

Multilayered electronic transfer tattoo that can enable the crease amplification effect

Lixue Tang, Jin Shang and Xingyu Jiang

Sci Adv 7 (3), eabe3778.
DOI: 10.1126/sciadv.eabe3778

ARTICLE TOOLS

<http://advances.science.org/content/7/3/eabe3778>

SUPPLEMENTARY MATERIALS

<http://advances.science.org/content/suppl/2021/01/11/7.3.eabe3778.DC1>

REFERENCES

This article cites 37 articles, 5 of which you can access for free
<http://advances.science.org/content/7/3/eabe3778#BIBL>

PERMISSIONS

<http://www.science.org/help/reprints-and-permissions>

Use of this article is subject to the [Terms of Service](#)

Science Advances (ISSN 2375-2548) is published by the American Association for the Advancement of Science, 1200 New York Avenue NW, Washington, DC 20005. The title *Science Advances* is a registered trademark of AAAS.

Copyright © 2021 The Authors, some rights reserved; exclusive licensee American Association for the Advancement of Science. No claim to original U.S. Government Works. Distributed under a Creative Commons Attribution NonCommercial License 4.0 (CC BY-NC).